ACS OMEGA

http://pubs.acs.org/journal/acsodf

Article

Effects of Mangosteen Peel Phenolic Compounds on Tilapia Skin Collagen-Based Mineralized Scaffold Properties

Eduardo P. Milan, Mirella R. V. Bertolo, Virginia C. A. Martins, César Enrique Sobrero, Ana M. G. Plepis, Thomas Fuhrmann-Lieker, and Marilia M. Horn*

Cite This: *ACS Omega* 2022, 7, 34022−34033

Read Online

ACCESS | Metrics & More | Article Recommendations | Supporting Information

ABSTRACT: A proper valorization of biological waste sources for an effective conversion into composites for tissue engineering is discussed in this study. Hence, the collagen and the phenolic compound applied in this investigation were extracted from waste sources, respectively, fish industry rejects and the peels of the mangosteen fruit. Porous scaffolds were prepared by combining both components at different compositions and mineralized at different temperatures to evaluate the modifications in the biomimetic formation of apatite. The inclusion of mangosteen extract showed the advantage of increasing the collagen denaturation temperature, improving the stability of its triple helix. Moreover, the extract provided antioxidant activity due to its phenolic composition, as confirmed by 2,2′-azino-bis(3-ethylbenzothiazoline-6-sulfonic acid) (ABTS) and 2,2-diphenyl-1-picrylhydrazyl (DPPH) antioxidant assays. Mineralization was successfully achieved as indicated by thermogravimetry and scanning electron microscopy. A higher temperature and a lower extract concentration reduced the calcium phosphate deposits. The extract also affected the pore size, particularly at a lower concentration. The X-ray diffraction pattern identified a low degree of crystallization. A high mineralization temperature induced the formation of smaller crystallites ranging from 18.9 to 25.4 nm. Although the deposited hydroxyapatite showed low crystallinity, the scaffolds are suitable for bone tissue applications and may be effective in controlling the resorbability rate in tissue regeneration.

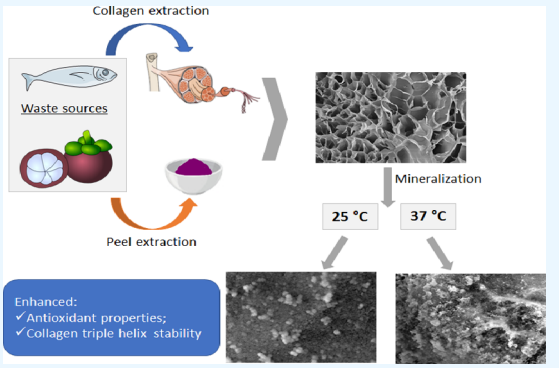

1. INTRODUCTION

Modern society is currently finding innovative alternatives for valorizing waste sources, minimizing disposal volumes, and eventually protecting the environment. Food waste has different definitions according to distinct countries and environmental agencies. A general description may be summarized as any byproduct from food production, processing, distribution, or consumption.[1] The valorization of waste sources in the production of value-added products represents a research field increasing in the last years, not only in the extraction and isolation of chemical compounds but also in biogas production.[2]

In many countries, an important source of food and incoming is found in fish production. In 2014, approximately 167 million tons of fish were produced from capture and aquaculture,[3] and such a high amount of fishery products reflects in a generation of vast quantities of residues.[4] Only 40% of the catch is used for consumption, while the other 60% is considered waste, arising in pollution due to the incorrect disposal of the organic material.[5] For that reason, efforts to deal efficiently with fish waste are necessary. In this study, we emphasize the valorization of fish processing waste as a source of compounds for the production of functional materials.

Fish skin is the major byproduct of the fish processing industry and a valuable collagen source. Even though mammalian animals, like pigs and cows, are traditional sources of this protein, freshwater byproducts are an alternative to outline religious reasons and potential risks of viral contamination, widespread issues when mammals are used.[6] Collagen is a dominant structural compound in fish skin, and it is responsible for the integrity of the extracellular matrix and connective tissues in the animal kingdom. To date, 29 different types of collagen with a specific amino acid sequence have been reported. The most common form is the collagen type I found in skin, tendon, and bone tissues. Collagen type I consists of three helical polypeptide chains with a repetitive sequence Gly-X-Y, where X and Y are generally occupied by proline (Pro) and hydroxyproline (Hyp).[7]

Natural phenolic compounds can interact with collagen through electrostatic and van der Waals forces. This strategy

Received: May 25, 2022
Accepted: August 23, 2022
Published: September 16, 2022

https://doi.org/10.1021/acsomega.2c03266
ACS Omega 2022, 7, 34022−34033

allows the combination of characteristics of both components and enhances specific properties of collagen materials, targeting different aims, such as their application in the reconstruction of damaged tissues. The xanthones found in the mangosteen (*Garcinia mangostana*) peel extract are potential phenolic compounds that can improve the antioxidant properties of the collagen scaffolds. Mangosteen is a tropical tree native to Southeast Asia and cultivated for its tart-sweet fruit. It is mainly valued for the use of its succulent pulp, while its pericarp portion, rich in xanthone compounds, is wasted. Thus, natural antioxidant compounds from mangosteen peel extract are a great source, as these active substances show various health effects.[8]

The anti-inflammatory action of α-mangostin, the majority phenolic compound found in mangosteen peel, is already known in the literature, mainly in treating rheumatoid arthritis.[9] Additionally, phenolic compounds delay or prevent free radical oxidation, which is responsible for damaging cells and tissues. Those oxidation processes are related to the first stages of carcinogenesis.[10] As the main application concerns tissue regeneration, the association of collagen and mangosteen provides a valuable material with antioxidant properties, with compounds that can scavenge free radicals and effectively accelerate the regeneration process.

The central feature of bone substitute materials is to exhibit properties that ideally result in total integration with natural bone tissue.[11] In this sense, designed scaffolds using inspiration from the complex hierarchical structure of bone are good candidates for bone tissue regeneration. In vertebrates, biomineralization is the process responsible for regulating and creating the skeleton's hierarchical structures.[12]

Mineralized collagen consists of collagen/hydroxyapatite (HA) hybrid composites and has been developed to mimic the natural structure of the bone. Unlike synthetic bone grafts that only act as a structural replacement, mineralized collagen scaffolds are bioabsorbable and osteoconductive, essential for tissue regeneration.[13] During the mineralization process, nucleation sites and intramolecular collagen spaces are essential for the nucleation and growth of the hydroxyapatite crystals. However, the method should be adequately chosen to prevent the denaturation of the protein and conservation of the triple helix structure, essential for biological interactions with natural tissue.

A few studies describe the *in vitro* mineralization of collagen extracted from marine and freshwater sources. In fact, a low denaturation temperature found in that collagen sources is a limitation for their use, demanding alternatives to produce stable collagen scaffolds at human body temperature.[14,15] We recently found that collagen phosphorylation of Tilapia fish skin increased the thermal stability of the protein triple helix structure and outlined the low denaturation temperature obstacle.[16] Nevertheless, even though an increase of about 7 °C in the denaturation temperature was observed, the stability achieved in the collagen fibers was insufficient to perform the mineralization process under body conditions.

Consequently, increased intramolecular interactions could also enhance the collagen triple helix stability. Therefore, the natural antioxidant compounds from mangosteen peel extract may actively perform that role by forming hydrogen bonds between the hydroxyl groups of xanthones and amino groups in the collagen. Then, the present study focuses on preparing *in vitro* mineralized fish collagen/hydroxyapatite scaffolds enriched with mangosteen extract, aiming at gathering the xanthones as potential antioxidant compounds and natural cross-linking agents.

2. MATERIALS AND METHODS

For the collagen type I source, random fresh skins of Nile Tilapia (*Oreochromis niloticus*) were collected from Pesque Pague Moinho (São Carlos, Brazil), and the mangosteen peel extract was obtained from mangosteen fruit (*G. mangostana*), acquired from a local market (São Carlos, Brazil). All chemicals were of analytical grade, purchased from Sigma-Aldrich, and used as received without any further purification.

2.1. Collagen Extraction and Characterization. The collagen was obtained as described earlier.[16] In summary, the fish skins were cleaned, scraped, and washed in 0.9 wt % saline solution and deionized water. After that, the fat content was removed with 1:1 acetone:ethanol solution and the samples were thoroughly washed with deionized water. The cleaned skins were submerged in a base solution for 48 h, followed by stabilization for 6 h in a sodium, potassium, and calcium sulfates and chlorides solution. The excess salt was removed with boric acid, deionized water, and ethylenediamine tetraacetic acid (EDTA). Acetic acid pH 3.5 was used for the collagen extraction, and the gel was neutralized with sodium hydroxide and then dialyzed against deionized water, followed by freeze-drying.

The collagen molecular weight was determined by sodium dodecyl sulfate polyacrylamide gel electrophoresis (SDS-PAGE), in the range of 130−150 kDa. Additionally, the α1/α2 ratio measured with optical densitometry confirmed that the extracted collagen is mainly Type I.[16]

2.2. Mangosteen Extraction and Characterization. The mangosteen peels were manually removed from the fruit, washed, dried, and milled. After sieving, the powder obtained was refluxed in a methanol/ethanol solution for 3 h, with further solvent evaporation and freeze-drying.[17] The mangosteen extract was characterized by its total phenolic content and antioxidant properties, using 2,2-diphenyl-1-picrylhydrazyl (DPPH) and 2,2′-azino-bis(3-ethylbenzothiazoline-6-sulfonic acid) (ABTS) radicals.

2.2.1. Folin−Ciocalteu Method. The total phenolic content (TPC) of mangosteen extract was determined according to the Folin−Ciocalteu colorimetric method, adapted for a 96-well microplate procedure.[17] Briefly, 50 μL of mangosteen peel extract (100 μg mL^{-1}) was mixed with 50 μL of Folin's reagent (Sigma-Aldrich); after 5 min, 200 μL of a sodium carbonate solution (20%, w/w) was added to the wells to alkalize the medium and form the blue phenolate anions. The absorbance was measured at 725 nm after 15 min in the dark, using a Thermo Scientific Multiskan GO UV−Vis spectrophotometer. A hydroethanolic solution (60%, v/v) was used as a blank, and gallic acid (Sigma-Aldrich) was used as standard ($y = 0.019x - 0.065$, R2 = 0.9997). The analysis was carried out in triplicate, and the result of mangosteen peel extract TPC was expressed in mg gallic acid equivalent (mg GAE) g^{-1} extract.

2.2.2. ABTS Antioxidant Assay. The 2,2′-azino-bis(3-ethylbenzothiazoline-6-sulfonic acid) (ABTS) radical antioxidant assay was conducted according to a procedure adapted from Re et al.[18] for a 96-well microplate. The radical was prepared by mixing a 14 mmol L^{-1} ABTS solution with a 4.9 mmol L^{-1} potassium persulfate solution for 15 h in the dark, followed by dilution in ethanol to adjust the absorbance at 734 nm. A hydroethanolic solution of mangosteen peel extract (20

https://doi.org/10.1021/acsomega.2c03266
ACS Omega 2022, 7, 34022−34033

μL, 25 μg mL^{-1}) was mixed with 180 μL of ABTS radical. The absorbance was measured at 734 nm after 10 min in a Thermo Scientific Multiskan GO UV−vis spectrophotometer. A hydroethanolic solution (60%, v/v) was used as a blank, and Trolox (6-Hydroxy-2,5,7,8-tetramethylchroman-2-carboxylic acid) (Sigma-Aldrich) was used as standard (y = 5.9013x + 3.3046, R2 = 0.9994). The % inhibition of mangosteen peel extract against ABTS radical was calculated according to eq 1

$$\%\ \text{inhibition} = \frac{(\text{Abs}_{\text{blank}} - \text{Abs}_{\text{extract}})}{\text{Abs}_{\text{blank}}} \times 100 \quad (1)$$

The analysis was carried out in triplicate, and the result was expressed as Trolox equivalent antioxidant activity (TEAC, μmol Trolox equivalent g^{-1} extract.)

2.2.3. DPPH Antioxidant Assay. The antioxidant activity of mangosteen peel extract was also evaluated against the 2,2-diphenyl-1-picrylhydrazyl (DPPH) radical, according to the method described by Pal et al.[19] and adapted for a 96-well microplate. DPPH solution (180 μL, 0.01 mmol L^{-1}) was placed to react with 20 μL of hydroethanolic solutions of mangosteen peel extract in different concentrations (3.125 to 100 μg mL^{-1}), diluted 15 × in each well. After 30 min, the absorbance was measured at 517 nm in a Thermo Scientific Multiscan GO UV−Vis spectrophotometer. The measurements were carried out in triplicate, and the % inhibition of the extract against the DPPH radical was calculated according to eq 1. By adjusting the curve of % inhibition versus the log of extract concentration,[20] it was possible to calculate IC_{50}, which corresponds to the concentration of mangosteen peel extract needed to inhibit 50% of the DPPH radical. Moreover, it was possible to determine the AAI,[21] that is, the antioxidant activity index of the extract, according to eq 2.

$$\text{AAI} = [\text{DPPH}] \times \text{IC}_{50} \quad (2)$$

2.3. Scaffolds Preparation and Mineralization. Collagen solution with a concentration of 3% (w/w) was prepared by dissolving the freeze-dried fish collagen in 0.5% (w/w) lactic acid, and the freeze-dried sample was used as the control scaffold, labeled COL.

Mangosteen extract (M) was added to collagen solution at concentrations of 10 and 30% in relation to the dry mass of the biopolymers. After the freeze-drying process, the samples were named CM10 and CM30, respectively.

The mineralization of the reference scaffold (COL) and the corresponding ones containing mangosteen extract (CM10 and CM30) was performed using the alternate immersion method,[22] with slight modifications. Briefly, the samples were immersed in 10 mL of 0.067 mol L^{-1} $CaCl_2$ solution buffered with 0.05 mol L^{-1} Tris buffer (pH 7.4) for 30 min, removed, washed with deionized water, and transferred to 10 mL of 0.04 mol L^{-1} Na_2HPO_4 solution (pH 9), for 30 min. The process was repeated three times. Finally, the scaffolds were rinsed with deionized water and freeze-dried.

Two different temperatures were employed for the mineralization process, 25 °C, and 37 °C. The scaffolds were identified with a suffix (25 or 37), corresponding to the temperature used in the process. Final mineralized samples were labeled: COL_25; COL_37; CM10_25; CM10_37; CM30_25; and CM30_37.

2.4. Scaffolds Characterization. *2.4.1. Attenuated Total Reflectance Fourier Transform Infrared Spectroscopy (ATR-FTIR).* For attenuated Total Reflectance Fourier transform Infrared spectroscopy, an ATR_FTIR Bruker α Platinum-ATR was used on a 4000−400 cm^{-1} interval with 24 scans and a resolution of 4 cm^{-1}. This method enables a quick, easy, and reliable analysis of the scaffolds.

2.4.2. Swelling Degree. Prior to the swelling test, the scaffolds COL, CM10, and CM30 were placed in a desiccator in the presence of NaOH(s) for 24 h. The dried scaffolds were weighed (dry weight) and placed in 5 mL of phosphate-buffered saline (PBS) pH 7.4. At predetermined times, the scaffolds were removed from the medium and weighed (wet weight), until achieve equilibrium (120 min). The process was carried out in triplicate. The swelling degree was calculated by eq 3.

$$\%\ \text{absorption} = \frac{\text{wet weight} - \text{dry weight}}{\text{dry weight}} \times 100 \quad (3)$$

2.4.3. Differential Scanning Calorimetry (DSC). DSC was used to study the thermal stability of the collagen in the scaffolds. The denaturation temperature characterizes the irreversible transformation of the native helical structure into uncoiled one, which means the loss of the structural integrity of the protein.[23] For this thermal profiling, a PerkinElmer DSC 7 was employed, in which the scaffolds (10 mg) were hermetically sealed in aluminum pans, and heated at 5 °C min^{-1} under a nitrogen atmosphere (90 mL min^{-1}). The collagen denaturation temperature was calculated using the inflection point of the thermal event.

2.4.4. Thermogravimetric Analysis (TGA). TGA was carried out using a PerkinElmer Pyris Diamond TG/DTA. Heating was performed in a platinum crucible in synthetic airflow (90 mL min^{-1}) at a rate of 10 °C min^{-1} from 30 to 700 °C. The sample weight was in the range of 9−10 mg. The residue at 700 °C determined the calcium phosphate content.

2.4.5. Scanning Electron Microscopy (SEM). SEM was employed to analyze the morphology and pore sizes of the scaffolds. The nonmineralized samples were placed in stubs and metalized in a Polaron Range metallizer at 1.10^{-1} mbar and pressure chamber of 20 mA, covering samples with a 12 nm platinum and analyzed in a Hitachi S-4000 at 9 kV. For mineralized samples a FEI-Quanta 250 FEG at 20 kV from the Werkstoffe des Bauwesens und Bauchemie, Universität Kassel, Germany was used without coating of samples. The ImageJ software was used to measure the pore size.

2.4.6. Mercury Intrusion Porosimetry (MIP). The porosity of the scaffolds was investigated by MIP with a Poremaster from Quantachrome (Boynton Beach, FL). The technique is based on using high pressure to force mercury into pore spaces, in which the required equilibrated pressure gives porosity properties, described by the ratio of cumulative of all pores in the scaffolds and the total volume of the sample.

2.4.7. Energy-Dispersive X-ray Spectroscopy (EDX). Mineralized scaffold composition was evaluated by their Ca/P content ratio using EDX semiquantitative measurement. A FEI-Quanta 250 FEG equipment from the Werkstoffe des Bauwesens und Bauchemie, Universität Kassel, Germany, was employed for the measurement.

2.4.8. X-ray Diffraction. X-ray diffractograms were performed in a Phillips PW 3710 MPD equipment, using Cu Kα radiation, 50 kV, 80 mA, rate scanning 2° min^{-1} and 2θ between 5 and 80°. Li et al.[24] described that the average size of the apatite crystallite (L) is calculated from the Scherrer equation (eq 4)

https://doi.org/10.1021/acsomega.2c03266
ACS Omega 2022, 7, 34022−34033

$$L = \frac{K}{\beta_m \cos\theta} \quad (4)$$

where L is the average crystallite size, λ is the wavelength of the X-radiation (1.54178 Å), K is a constant related to the crystallite shape, β_m is the full width of the peak at half-maximum (FWHM), and θ is the diffraction angle of the chosen peak (plane 002 reflection).

The degree of crystallinity (X_c) expresses the fraction of the crystalline apatite phase and was assessed using eq 5

$$X_c\ (\%) = \left(\frac{0.24}{\beta_{002}}\right)^3 \quad (5)$$

where X_c is the degree of crystallinity, β_{002} is the FWHM of the 002 plane reflection, and 0.24 is a constant found for many HA powders.[25]

Scaffolds pore size and Ca/P ratio on mineralized samples values were statistically treated using analysis of variance (ANOVA) and Tukey's test on Origin software with a significance level set at 5%.

3. RESULTS AND DISCUSSION

3.1. Mangosteen Extract Characterization. The total phenolic content is a useful measure of the antioxidant power and the reducing activity of a plant extract. It quantitatively determines polyphenols, molecules that act as primary antioxidants and as free radical reducers, being responsible for most of the antioxidant activity attributed to plants and their derivatives.[26,27] The TPC of the mangosteen peel extract obtained by a methanol/ethanol (70:30) extraction is shown in Table 1. A value of about 112 mg GAE g^{-1} mangosteen peel extract was determined, consistent with that found in the literature for mangosteen peel and pericarp extracts, obtained by various extraction methods and using different solvents. Suttirak and Manurakchinakorn[28] evaluated the TPC of mangosteen peel extracts obtained in different concentrations of ethanol and water. The extract with the highest TPC was obtained with the 50:50 mixture, presenting 152.52 mg GAE g^{-1} extract, a value close to that determined in this study. The mangosteen peel extract obtained by Chaiwarit et al.[29] from microwave-assisted extraction (MAE), with a 60:40 ethanol/water mixture, presented about 143.6 mg GAE g^{-1} of dry matter (DM), a value higher than that brought by Wittenauer, Schweiggert-Weisz, and Carle[27] for the mangosteen pericarp extract obtained by extraction with ethanol/water (50:50) (85.4 mg GAE g^{-1} DM).

Table 1. Total Phenolic Content (TPC) and Antioxidant Activity against ABTS and DPPH Radicals for Mangosteen Peel Extract

TPC (mg GAE g^{-1} extract)	112.05 ± 5.27
TEAC[a] (μmol Trolox equivalent g^{-1} extract)	2330.56 ± 81.08
IC_{50}[b] ($\mu g\ mL^{-1}$)	8.74
AAI[a]	2.75

[a]Determined by the ABTS antioxidant assay. [b]Determined by the DPPH antioxidant assay.

It is worth noting that the phenolic content of a plant extract is a specific value for each product, with no "correct" quantity to be determined since there are several factors, intrinsic and extrinsic, that can affect this property: the fruit ripening stage (the TPC of the mangosteen peel tends to decrease according to the maturation progress), the polarity of the solvent used during the extraction process (more polar solvents tend to extract a higher content of polyphenols from mangosteen peel extract), and the variables of the extraction process adopted (sample pretreatment, solid/liquid ratio, the proportion between the solvents used, microwave or ultrasound assistance, stirring, among others).[26,28,29]

The ABTS antioxidant assay provides a measurement of the antioxidant power of mangosteen extract by the discoloration of the ABTS radical at 734 nm. The average value of Trolox obtained for a 25 $\mu g\ mL^{-1}$ hydroethanolic solution of mangosteen peel extract was 5.83 ± 0.20 $\mu mol\ L^{-1}$, corresponding to an average inhibition of 37.69 ± 1.20% of the ABTS radical. The result of the inhibitory power of the extract against the radical can be expressed as Trolox equivalent antioxidant activity (TEAC), corresponding to 2330 ± 81 μmol Trolox equivalent g^{-1} mangosteen peel extract (Table 1). The ethanolic and methanolic extracts from the mangosteen pericarp obtained by Zarena and Sankar[26] showed maximum activity (100% inhibition) of 34.95 and 31.25 $\mu mol\ L^{-1}$ Trolox equivalent at 100 $\mu g\ mL^{-1}$ of extract. Wittenauer, Schweiggert-Weisz, and Carle,[27] in turn, obtained a value of 1063.69 μmol of Trolox equivalent g^{-1} of mangosteen pericarp extract.

Regarding the inhibition results against the DPPH radical, the mangosteen peel extract showed an IC_{50} of 8.75 $\mu g\ mL^{-1}$, the concentration necessary to stabilize 50% of the DPPH radical by the donation of the hydrogens from the hydroxyl groups of the phenolics present in the extract. The results imply that the mangosteen peel extract can act as a primary antioxidant, reacting and stabilizing free radicals such as DPPH by hydrogen donation. Zarena and Sankar[26] also calculated the IC_{50} for mangosteen pericarp extracts obtained with different solvents. The methanolic extracts presented, respectively, IC_{50} of 52.62 and 69.43 $\mu g\ mL^{-1}$, superior to those of acetone, ethyl acetate, and water/acetone extracts. Indeed, the higher the IC_{50}, the greater the amount of extract required for the 50% inhibition of DPPH. The extract obtained from the mangosteen peel with a 70:30 methanol/ethanol mixture in this study showed a higher antioxidant activity value than all of the pericarp extracts obtained.[26]

The IC_{50} value can also be used to calculate the antioxidant activity index of the extract (AAI), determined by specific ranges. In fact, AAI < 0.5 indicates low antioxidant activity, between 0.5 and 1.0 represents moderate antioxidant activity, between 1.0 and 2.0 indicates strong antioxidant activity, and greater than 2.0 represents very strong.[21] The antioxidant activity calculated for mangosteen peel extract in this study (AAI = 2.75) reinforces the aim of its addition, that is, to incorporate a plant extract rich in polyphenolic compounds to improve the active properties of collagen scaffolds.

3.2. Scaffolds Characterization. The main task of tissue engineering scaffolds is to mimic the function of the extracellular matrix, providing appropriate design parameters on the essential structural, physicochemical, and composition properties. Considering the change in scaffold composition and mineralization conditions, like temperature, variation of properties could be achieved. Consequently, properties like pore size, mineralization amount, and crystallinity of the inorganic deposit are evaluated in this study.

3.2.1. ATR-FTIR. The bands for nonmineralized samples (Figure S1-Sn) allow the identification of amides A and B

https://doi.org/10.1021/acsomega.2c03266
ACS Omega 2022, 7, 34022−34033

(3272−3240 and 2940−3080 cm^{-1} regions) and amides I, II, and III found in the ranges of 1700−1600, 1532−1555, and 1240 cm^{-1}, respectively, all corresponding to collagen.[30] Mangosteen extract characteristic bands were previously described at 1640 cm^{-1} from C═O stretching vibration and at 1450 cm^{-1} from skeletal C═C aromatic vibration.[31] When incorporated into collagen scaffolds, the extract bands overlap the collagen ones, making them indistinguishable. Nevertheless, no notable alteration or shifting in the band positions was observed, indicating that electrostatic forces purely cause the interaction between both components.

FTIR spectra of the mineralized samples obtained at both temperatures and different collagen/mangosteen compositions are shown in Figure 1. Bands at around 1020 cm^{-1} and

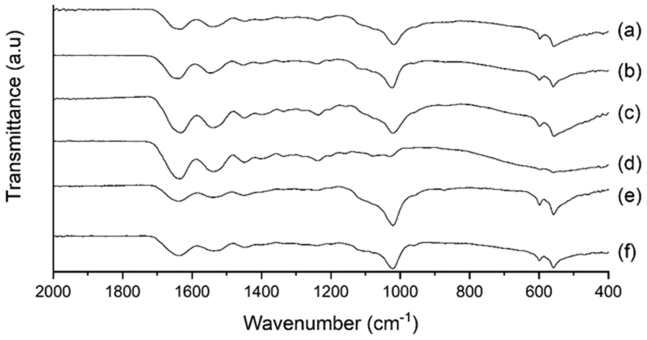

Figure 1. FTIR spectra for (a) COL_25; (b) COL_37; (c) CM10_25; (d) CM10_37; (e) CM30_25; and (f) CM30_37.

between 560 and 600 cm^{-1}, characteristics from PO_4^{3-} vibrational stretching and deformational vibration, respectively, are observed.[32] All of those bands are associated with phosphate salt formation, the first indicator of the successful mineralization process. The finding bands from phosphate in all mineralized samples showed that the composition and mineralization temperature did not interfere with the deposit of these inorganic salt in the scaffolds. Consequently, all of the samples were considered for further characterization.

As previously stated, the presence of amides I, II, and III are characteristic of collagen triple helix, and its stability can be calculated by the ratio of amide III peak (1240 cm^{-1}) and the peak at 1450 cm^{-1}, associated with the proline/hydroxyproline C−H bond of the pyrrolidine ring (Table S1-Sn). Both bands are sensitive to structural changes in the protein backbone chain, in which a ratio close to 1 implies collagen structural integrity. Ratio values closer to 0.5 indicate a triple helix rupture, the once ordinated tripe helix is randomly coiled, and all of the biological properties of collagen are missed.[33]

Evaluating the stability and existence of collagen triple helix structure in the scaffolds is essential for tissue engineering applications. In fact, the helicoidal form is involved in the biological recognition process, as specific triple-helical domains are identified as cell adhesion sites.[34] The determined 1240/1450 cm^{-1} ratio showed values ranging from 0.96 to 1.06, indicating the structural integrity of the collagen in the scaffolds.

3.2.2. Swelling Degree. The resulting reference scaffold (COL) and the corresponding ones containing mangosteen extract (CM10 and CM30) were monitored by measuring changes in their weight over time when incubated in a PBS medium. The determined swelling ability was observed in all of the scaffolds and reached equilibrium within 2 h, without dissolution of the sample at the end of the experiment (Figure S2-Sn). All scaffolds swelled rapidly in contact with PBS, and the absorption of the buffer depends on the presence and concentration of mangosteen. The equilibrium swelling after 2 h was 1180 ± 35% (COL), 646 ± 31% (CM10), and 484 ± 23% (CM30). The reduction of swelling percentage is directly associated with an increase in the intramolecular interactions between the collagen and the mangosteen extract incorporated in the scaffolds. Indeed, it is known that the swelling capacity of a polymer network depends on the degree of cross-linking.[35] Therefore, the swelling tests confirmed the presence of a high amount of interactions between collagen and the phenolic compound, and the observed behavior is concentration-dependent.

3.2.3. Differential Scanning Calorimetry (DSC). Collagen is composed of amino acid chains that fold into a triple helix structure. As discussed before, its unique property is necessary for tissue engineering materials. At the denaturation temperature (Td), the once ordinated triple helix is turned into an unwinder form, and random chains are observed.[23]

The denaturation temperature involves the rupture of interchain hydrogen bonds and correlates to chain mobility. Collagen modifications, like cross-linking process or the addition of stable inorganic compounds, modify the network architecture, affecting the triple helix stability.[23] Indeed, a higher Td means a stronger interchain bonding between the collagen chains. Fish skin typically provides collagen with lower Td than mammalian ones, limiting the use and processability of scaffolds prepared with those sources. Thus, enhancing this property is beneficial and desirable for the target application.

Due to the low heat flow associated with the collagen denaturation thermal transition, mineralized scaffolds prepared at both temperatures did not show an inflection point in DSC measurements, characteristic of this conversion of the protein conformation. This behavior is probably associated with the high calcium phosphate deposits in the scaffolds. Nevertheless, the FTIR analysis showed a stable collagen conformation for these samples.

The control collagen sample (COL) showed a Td of 33.5 °C (Figure 2a), a comparable value also described for collagen

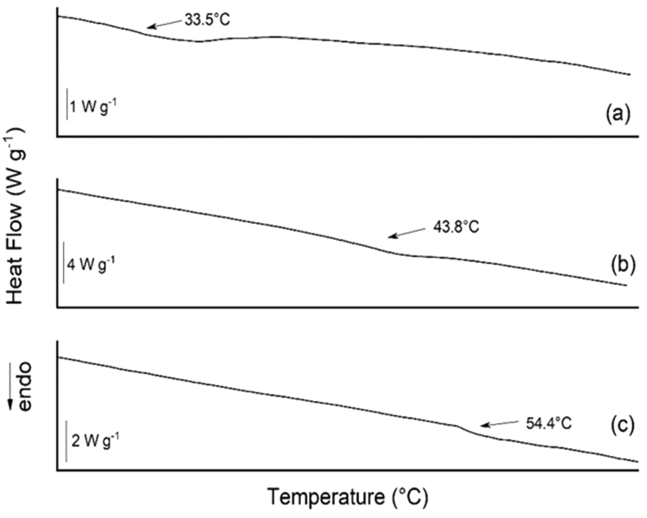

Figure 2. DSC curves of the scaffolds: (a) COL, (b) CM10, and (c) CM30.

https://doi.org/10.1021/acsomega.2c03266
ACS Omega 2022, 7, 34022−34033

Table 2. Percentage of Weight Loss at Different Temperature Ranges, Residue Percentage, and T_{onset} Obtained through TGA

	% weight loss				
scaffold	30−200 °C	200−500 °C	500−700 °C	%residue (700 °C)	T_{onset} (°C)
COL	8.34	63.16	27.54	0.96	237.42
CM10	18.17	62.63	17.82	1.38	274.12
CM30	13.47	57.12	28.59	0.29	283.30
COL_25	8.41	50.12	23.79	17.68	258.55
COL_37	7.60	53.69	30.99	7.72	251.01
CM10_25	9.11	52.60	17.67	20.62	267.39
CM10_37	9.84	51.00	31.77	7.38	269.90
CM30_25	7.37	56.61	25.40	10.61	256.52
CM30_37	6.44	52.70	30.17	10.69	254.64

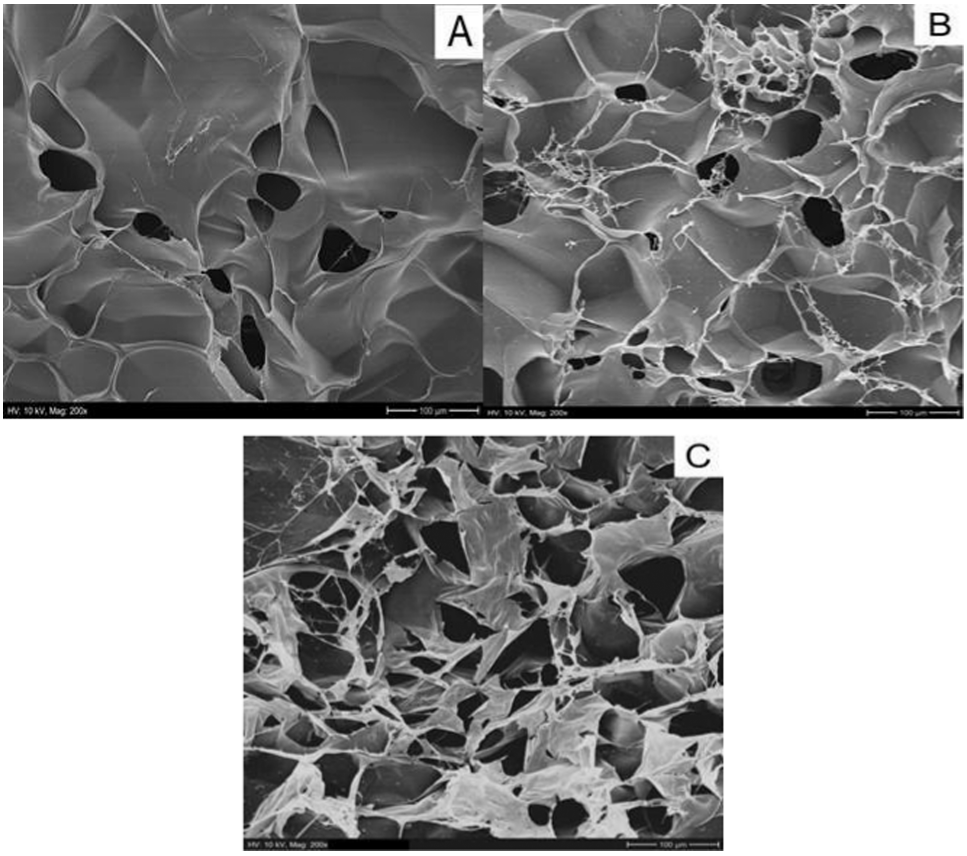

Figure 3. SEM surface images of the scaffolds: (A) COL, (B) CM10, and (C) CM30.

extracted from scales of the marine fish barramundi (*Lates calcarifer*), of 36.4 °C.[36] The mangosteen addition increased the temperature to 43.8 °C (CM10, Figure 2b) and 54.4 °C (CM30, Figure 2c). As the extract concentration directly relates to high triple helix stability, we conclude that its presence increases the number of hydrogen bonds formed in the collagen network.[37] Indeed, mangosteen extract is rich in xanthones compounds that can raise the number of linkages, reflecting an increase of Td. It is important to note that its addition did not interfere with the triple-helical structure of collagen.

3.2.4. Thermogravimetry. TGA analysis assesses the thermal stability and the weight loss steps associated with weight change when the scaffolds are heated at a constant rate. Additionally, it allows determining the deposit calcium phosphate content by analyzing the residue value.

All of the samples, mineralized or not, showed the same pattern of weight loss percentage, divided into three steps (Figures S3-Sn and S4-Sn). The first step (30−200 °C range), related to the moisture content, is the initial break of inter and intramolecular along with hydrogen bonds, releasing the surrounding water molecules and disrupting the collagen triple helix. Degradation of polymeric chains occurred in the second step (200−500 °C), while the third step (500−700 °C) was associated with organic carbonization. The remaining residue is associated with the inorganic deposits obtained by the *in vitro* mineralization process. The weight loss percentage values in each step are given in Table 2.

In general, all of the scaffolds showed a similar weight loss percentage associated with the first step, except for those prepared with mangosteen extract and not mineralized (CM10 and CM30). The difference might be related to the xanthones cross-linking effect in the collagen, reflecting more hydrating

https://doi.org/10.1021/acsomega.2c03266
ACS Omega 2022, 7, 34022−34033

Table 3. Pore Size, Porosity for All Scaffolds and Ca/P Ratio, Crystallite Size, and Crystallinity Degree for the Scaffolds[a]

scaffold	pore size (μm)	porosity (%)	Ca/P ratio ± SD	crystallite size (nm)	degree of crystallinity (%)
COL	85.0 ± 7.4^{d}	110.4	-	-	-
CM10	83.8 ± 22.9^{d}	101.3	-		-
CM30	103.4 ± 8.8^{c}	101.1	-	-	-
COL_25	142.3 ± 16.5^{b}	96.2	1.68 ± 0.11^{a}	31.5	0.697
COL_37	30.8 ± 4.1^{e}	93.1	1.64 ± 0.04^{a,b}	25.4	0.367
CM10_25	241.8 ± 33.1^{a}	89.9	1.56 ± 0.05^{b,c}	36.7	1.107
CM10_37	18.3 ± 14.9^{e}	98.4	1.52 ± 0.04^{c}	18.9	0.150
CM30_25	29.6 ± 1.9^{e}	87.1	1.61 ± 0.16^{a,b,c}	38.9	1.314
CM30_37	31.6 ± 2.6^{e}	90.3	1.55 ± 0.09^{b,c}	23.6	0.294

[a]Same letter in the column means no significant difference; significance level of 5%.

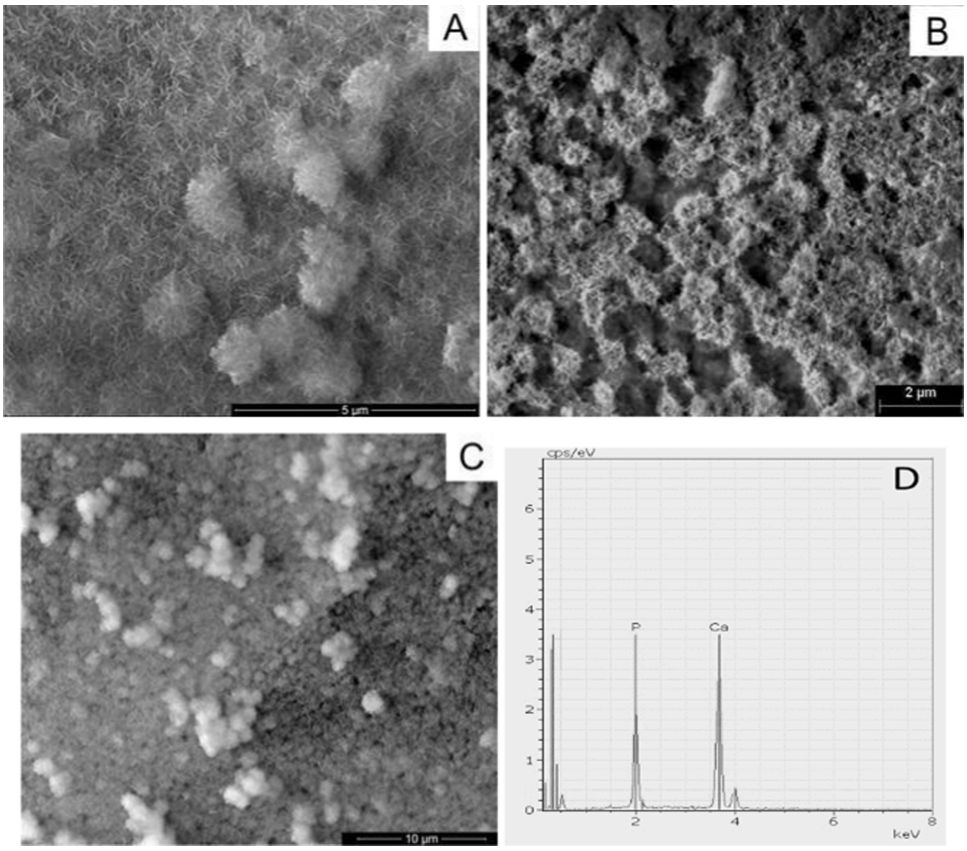

Figure 4. SEM surface images of the scaffolds mineralized at 25 °C: (A) COL_25, (B) CM10_25, and (C) CM30_25. Image D emphasizes the EDX result for the CM30_25 scaffold.

water molecules due to an increasing number of OH groups. The same effect was not observed for the mineralized samples since calcium phosphate deposits act as a steric hindrance, reducing the amount of hydrating water molecules.

The residue content related to the apatite deposits increased in the mineralized samples compared to those nonmineralized. The chosen mineralization temperature affected the quantity of observed residue, as noted for the scaffolds prepared with collagen and low mangosteen extract concentration. In both cases, a reduction of about 35% (COL_25 and COL_37) and 43% (CM10_25 and CM10_37) was achieved when the temperature used in the mineralization process increased from 25 to 37 °C. In fact, COL and CM10 scaffolds displayed lower Td values (33.5 and 45.3 °C, respectively), as observed by DSC measurements.

The CM30_25 and CM30_37 scaffolds revealed similar mineral deposition percentages. These results are associated with high thermal stability, as CM30 showed a higher Td value (54.4 °C), indicating a high resistance to temperature conditions in the mineralization procedure. Although fewer mineral deposits were obtained, the presence of a high amount of mangosteen maintains the collagen fibrils stable, allowing the deposition of a comparable amount of calcium phosphate. This lower amount is related to the high cross-linking network formed in the samples, which leads to a few binding sites to calcium phosphate. Compared to the collagen-phosphorylated samples previously prepared,[16] the amount of mineral deposited is lower. Indeed, the presence of phosphate groups in the collagen structure serves as new nucleation sites for apatite formation inside the collagen fibers, and consequently, that approach increases the calcium phosphate precipitation.[37] Nevertheless, even though phosphorylation assists the increase in the mineral amount, it does not improve enough collagen

https://doi.org/10.1021/acsomega.2c03266
ACS Omega 2022, 7, 34022−34033

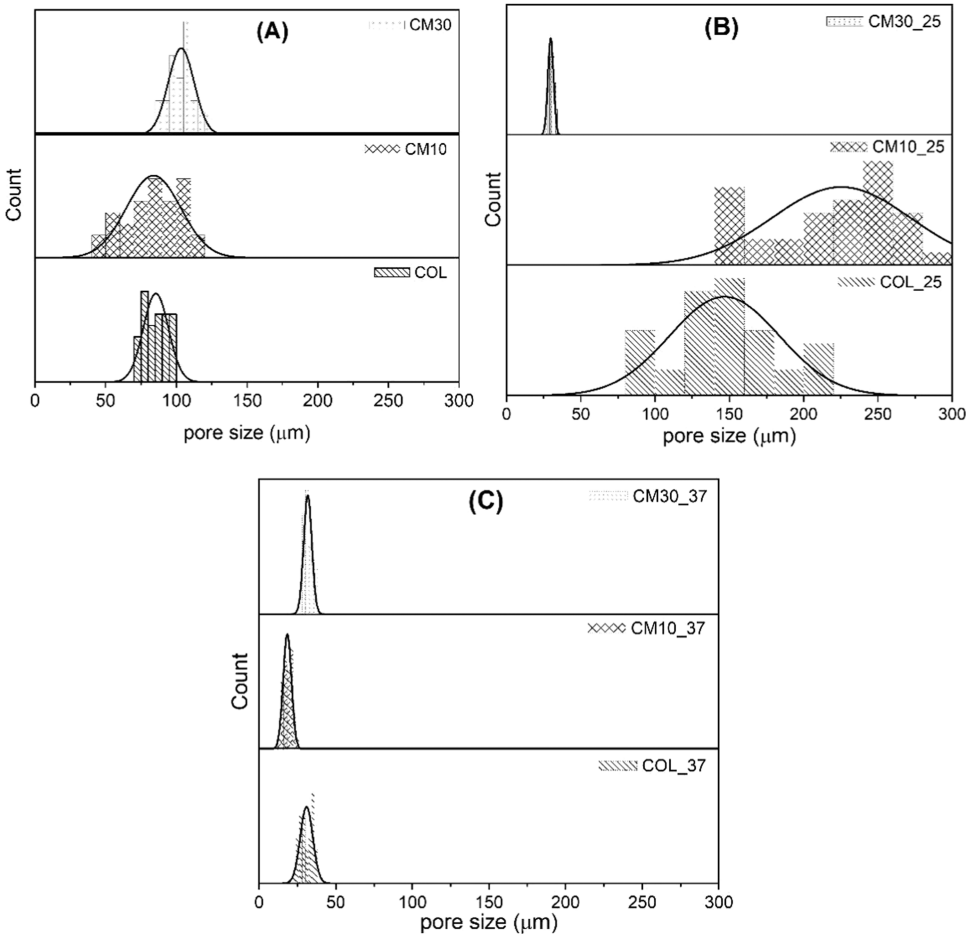

Figure 5. Pore size distribution for scaffolds: (A) nonmineralized, (B) mineralized at 25 °C, and (C) mineralized at 37 °C.

triple helix stability. This feature is achieved by inserting the mangosteen extract into the scaffolds.

The inclusion of mangosteen extract in the collagen scaffolds had a favorable effect on thermal stability, as the thermodegradation onset temperature increased by about 36 to 45 °C compared to the sample control (COL). Likewise, the mineralization process increased the thermal stability of the collagen scaffolds, as the calculated onset was 258.55 °C (COL_25) and 251.01 °C (COL_37). On the other hand, the thermal stability decreased after the mineralization in the scaffolds containing mangosteen extract, as onset temperature values ranged from 254.64 °C (CM30_37) to 269.90 °C (CM10_37).

3.2.5. Scanning Electron Microscopy (SEM). The distribution and size of pores, porosity, and geometry of the scaffolds are essential parameters for the materials used in tissue engineering. Furthermore, pore interconnectivity and pore wall morphology influence cell seeding, migration, mass transport, growth, gene expression, and consequently the formation of new tissue.[38] An approach usually applied for surface pores is directly measuring its structure in the SEM images. The main advantage of this method consists of both precise visualization at high resolution and availability.

Fish skin collagen scaffold presented porous structures homogeneously distributed on the surface area with interconnected pores (Figure 3a), and the inclusion of mangosteen extract did not change the existence of pores in the scaffold (Figure 3b,c). The control sample (COL) exhibited a pore size of 85.0 ± 7.4 μm (Table 3), and the extract concentration influenced pore size values. For the CM10 sample, the calculated pore size did not change compared to the control sample, while the addition of the highest extract concentration enlarged the pore size up to 103.4 ± 8.8 μm (CM30).

SEM images of mineralized scaffolds indicated the deposit of inorganic minerals on the surface of all of the samples, and the observed behavior was independent of the extract concentration or the temperature, demonstrating the effectiveness of mineralization. The morphology of calcium phosphate crystals observed in the scaffolds was spherical clusters with needle-shaped crystals (Figures 4 and S5-Sn).

In the absence of mangosteen, the temperature used in the mineralization process influenced the calculated pore size, decreasing from 142.3 ± 16.5 μm (COL_25) to 30.8 ± 4.1 μm (COL_37). For samples containing 10% of mangosteen extract, the same behavior was noted, as CM10_25 showed a pore size value of 241.8 ± 33.1 μm, while CM10_37 showed 18.3 ± 14.9 μm (Table 3). The amount of deposit calcium phosphate is probably related to the observed behavior. TGA measurements of COL_25 and CM10_25 scaffolds revealed higher residue values than those samples with the same composition but mineralized at 37 °C.

Oppositely, the scaffolds prepared with the highest extract concentration (CM30_25 and CM30_37) showed a similar pore size of around 30 μm (Table 3), assuming that the temperature does not influence that characteristic in the

https://doi.org/10.1021/acsomega.2c03266
ACS Omega 2022, 7, 34022−34033

analyzed samples. Interestingly, these scaffolds displayed the same amount of calcium phosphate (around 10.6%), calculated by TGA. With these findings, we concluded that the temperature influences the characteristics of the scaffolds in the absence of the extract or when its concentration is low. Differently, at high mangosteen concentration, the temperature has low or even no influence on the properties of the scaffolds, probably by the high stability of collagen chains provided by the extract addition.

It is a consensus that different pore sizes are involved in the maturation of distinct tissues in the body. For example, for neovascularization, a pore size of 5 μm is needed, while pores between 10−75 μm allow penetration of fibrous tissue. Pores of 75−100 μm are required for osteoid tissue growth and larger pores (100−350 μm) for bone regeneration.[39,40] Consequently, all of the scaffolds prepared in this study are suitable for tissue engineering applications.

Additionally, a comparison of pore size distribution as a function of mangosteen extract concentration can be performed (Figure 5).

For nonmineralized samples (Figure 5A), an increase in pore size characteristics was observed, but the obtained values were not statistically different. The mangosteen extract concentration (Figure 5B) strongly affected the property in scaffolds mineralized at 25 °C, as in its absence or low concentration, large pore sizes, and wide distribution was obtained. On the contrary, a small pore size with a narrow distribution was noted in Figure 5C. Thus, the samples prepared under these experimental conditions showed a similar quantity of phosphate deposits, ranging from 7.4 to 10.7% (Table 2), probably connected to the comparable pore size.

3.2.6. Mercury Intrusion Porosimetry (MIP). Different characterization techniques can be employed for the size and quantity of pores evaluation. Still, not all are sensitive to distinguishing between pores, blind pores (dead-end or saccate), or closed pores. A method that uses a nonwetting liquid penetration to measure the size and volume of pores is an alternative manner of calculating the porosity of scaffolds. The porosity results reflect the evaluation of interconnectivity characteristics in the scaffolds.[40]

The porosity of scaffolds was calculated by the mercury intrusion porosimetry test, and the results are given in Table 3. The values ranged from 87 to 110%, and mangosteen extract addition slightly decreased porosity property. Furthermore, mineralization also induced a decrease in porosity without, however, leading to a collapsed structure regardless of the temperature used in the process. The values above 100% observed for the nonmineralized samples might be related to the applied pressure for mercury inclusion that forces a decrease in the volume sample. It is known that an appropriate scaffold microstructure with porosity values of about 80 to 90% is a remarkable feature for tissue engineering applications, as this range provides enough space for nutrients and gas exchange and cell proliferation and fixation, including bone cells.[41] Then, the mineralization process not only provides a first signal recognition to induce bone tissue growth but also contributes to obtaining scaffolds with appropriate porosity characteristics. Al-Munajjed and O'Brien[42] described a similar pattern for collagen scaffolds prepared with a bovine tendon, as the mineralization process reduces the porosity of the samples.

3.2.7. Energy-Dispersive X-ray Spectroscopy (EDX). The EDX analysis confirmed the presence of calcium and phosphorous on the surface of the scaffolds, as exemplified by the standard pattern in Figure 6D. The stoichiometric ratio of Ca/P for crystalline hydroxyapatite (HA) was 1.67, a stable

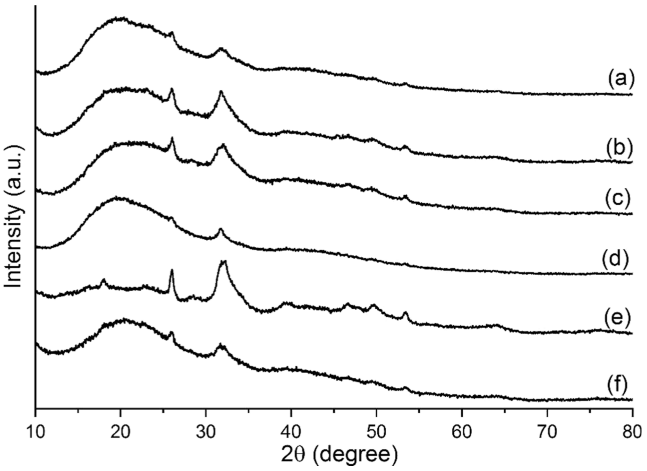

Figure 6. X-ray diffraction patterns of mineralized scaffolds: (a) COL_25, (b) CM10_25, (c) CM30_25, (d) COL_37, (e) CM10_37, and (f) CM30_37.

and low soluble phosphate form. The Ca/P ratio is an important parameter that characterizes calcium phosphate inorganic ceramics. The calculated values range from 1.52 ± 0.04 (CM10_37) to 1.68 ± 0.11 (COL_25), depending on the extract concentration and the temperature applied in the mineralization process (Table 3). Ca/P ratios lower than 1.67, as observed for the CM10_37, suggest that the calcium phosphate can be classified as calcium phosphate deficient in calcium.[43] Even though some of the scaffolds displayed values below the theoretical HA one, it does not mean they are not feasible for the target application. The obtained calcium phosphate deficient in the calcium phase is similar to the ratio found in human bone in the initial mineralization phase.[44] That HA phase shows a high solubility and can easily participate in the maturation and growth of the new bone tissue.

3.2.8. X-ray. The mineralized scaffolds were examined by X-ray diffraction. Diffractograms for the mineralized scaffolds showed a broad peak for collagen at approximately 20°, along with peaks for calcium phosphate comparable to noncrystalline HA (Figure 6). No other calcium salts or phosphates were detected according to JCPDS 9-0432. Additionally, the HA characteristics peaks were observed at 25.94, 31.84, 39.38, 46.63, and 49.50° (2θ) corresponding to the 002, 211, 310, 222, and 213 crystallographic plans. The peaks showed a wide pattern resulting from the small size and low crystallinity of the HA deposited during the mineralization. Nevertheless, the findings are similar to the HA characteristics found in the mineral phase of natural bone.[45] The dimensions of apatite crystals are described in the literature. Even though different values are reported, they usually are a nanometric scale, ranging from 30 to 50 nm (length), 15 to 30 (width), and 2 to 10 nm (thickness).[46]

The diffraction peak 002 measured the crystalline grain size of the calcium phosphate deposited in the scaffolds. Scherrer's equation (eq 4) was applied to calculate the crystallite size (Table 3). Different behavior was noted in the size of HA when mineralization temperature and the inclusion of mangosteen extract were varied. At 25 °C, the experimental

https://doi.org/10.1021/acsomega.2c03266
ACS Omega 2022, 7, 34022−34033

condition induced hydroxyapatite formation with crystallite sizes between 31.5−38.9 nm, increasing due to rising extract concentration. Oppositely, at 37 °C, the mineralization induced the formation of smaller crystallites that range from 18.9 to 25.4 nm, with a reduction of this characteristic. Crystal size values agree with those reported previously by other authors. Wang and Liu[43] developed composites with bovine collagen deposition of hydroxyapatite and suggested that the crystallite size range of HA was 10−30 nm. Wan et al.[47] found crystallite sizes of 37 and 46 nm for the HA crystals formed in the bacterial cellulose. Rusu et al. observed a crystallite size range of 15−50 nm on a chitosan matrix.[25] Besides, Elhendawi et al.[48] prepared Chitosan/HA nanocomposites using in situ coprecipitation technique and obtained a crystallite size of about 15−21 nm.

Besides, the degree of crystallinity calculated by eq 5 ranged from 0.294 to 1.314, as compiled in Table 3. Lower values are obtained for the high employed mineralization temperature, and the mangosteen concentration affected only the property of scaffolds mineralized at 25 °C. However, a previous study reported an increased size of the crystallite and the degree of crystallinity at high temperatures.[48] Although the deposited HA shows crystallinity values close to 1, which means low crystallinity properties, the obtained scaffolds are suitable for bone tissue applications. Hydroxyapatite with these characteristics controls the resorbability rate in tissue regeneration.[46]

4. CONCLUSIONS

Waste sources are good alternatives for extracting valuable compounds and applying them to tissue regeneration. This study proved that agro-industrial waste and the discard of the aquatic processing industry are appropriate sources of phenolic compounds and collagen, respectively. The mangosteen peel can be considered a bioactive source by its antioxidant properties, as confirmed by the ABTS and DPPH antioxidant assays with comparable values to the literature. Its incorporation in the collagen scaffolds provides functional prevention of the free radicals oxidation process. The integrity of the triple helix of collagen was preserved during its extraction, as confirmed by FTIR spectroscopy. Moreover, the increase in extract concentration led to a high stabilization of the protein molecule, as demonstrated by the rise in Td values.

All of the scaffolds showed a highly porous structure, demonstrating that the introduction of the mangosteen extract and mineralization had no negative effect on this parameter. Its features play an essential role in calcium phosphate nucleation, as pores and porosity are considered key characteristics for tissue engineering scaffolds.

Diverse behavior was observed as an effect of composition and mineralization temperature on scaffold properties. In general, similar characteristics like calcium phosphate, pore size, and porosity were noted in the absence of extract and at a lower concentration. On the contrary, at a high mangosteen content, the temperature had only a marginal influence on the properties of the scaffolds, probably due to the high stability of collagen chains provided by the extract addition.

Thus, the scaffolds could contribute to the formation of bone tissue, as the HA crystallites deposited in the mineralization process have similar characteristics to the calcium phosphate phase found in human bone in the initial mineralization process. Additionally, the low degree of crystallinity infers that it can be reabsorbed *in vivo*.

■ ASSOCIATED CONTENT

Supporting Information

The Supporting Information is available free of charge at https://pubs.acs.org/doi/10.1021/acsomega.2c03266.

FTIR spectra for COL, CM10, and CM30 (Figure S1-Sn); TGA curves for COL, CM10, and CM30 (Figure S2-Sn); TGA curves for COL_25, (b) COL_37, (c) CM10_25, (d) CM10_37, (e) CM30_25, and (f) CM30_37 (Figure S3-Sn); SEM surface images of the scaffolds mineralized at 37 °C: COL_37, CM10_37, and CM30_37, and the EDX result for the CM30_37 scaffold (Figure S4-Sn); and FTIR band intensity ratio of 1240 and 1450 cm^{-1} bands (Table S1-Sn) (PDF)

■ AUTHOR INFORMATION

Corresponding Author

Marilia M. Horn − *Physical Chemistry of Nanomaterials, Institute of Chemistry and Center for Interdisciplinary Nanostructure Science and Technology (CINSaT), University of Kassel, Kassel 34132, Germany;* orcid.org/0000-0002-5133-4954; Email: mhorn@uni-kassel.de

Authors

Eduardo P. Milan − *Interunits Graduate Program in Bioengineering (EESC/FMRP/IQSC), University of São Paulo (USP), São Carlos 13566-590, Brazil; Physical Chemistry of Nanomaterials, Institute of Chemistry and Center for Interdisciplinary Nanostructure Science and Technology (CINSaT), University of Kassel, Kassel 34132, Germany*

Mirella R. V. Bertolo − *São Carlos Institute of Chemistry, University of São Paulo (USP), São Carlos 13566-590, Brazil*

Virginia C. A. Martins − *São Carlos Institute of Chemistry, University of São Paulo (USP), São Carlos 13566-590, Brazil*

César Enrique Sobrero − *Institute of Materials Engineering, University of Kassel, Kassel 34125, Germany*

Ana M. G. Plepis − *Interunits Graduate Program in Bioengineering (EESC/FMRP/IQSC), University of São Paulo (USP), São Carlos 13566-590, Brazil; São Carlos Institute of Chemistry, University of São Paulo (USP), São Carlos 13566-590, Brazil*

Thomas Fuhrmann-Lieker − *Physical Chemistry of Nanomaterials, Institute of Chemistry and Center for Interdisciplinary Nanostructure Science and Technology (CINSaT), University of Kassel, Kassel 34132, Germany;* orcid.org/0000-0003-3473-534X

Complete contact information is available at: https://pubs.acs.org/10.1021/acsomega.2c03266

Author Contributions

E.P.M. contributed to conceptualization, methodology, formal analysis, investigation, and writing—original draft. M.R.V.B. involved in methodology, investigation, formal analysis, and writing—original draft. V.C.A.M. contributed to conceptualization, methodology, formal analysis, and writing—original draft. A.M.G.P. contributed to conceptualization, resources, supervision, and writing—review & editing. C.E.S. performed investigation. T.F.-L. contributed to resources, supervision, and writing—review & editing. M.M.H. involved in methodology,

https://doi.org/10.1021/acsomega.2c03266
ACS Omega 2022, 7, 34022−34033

formal analysis, supervision, and Writing—original draft and review & editing.

Funding

This work was supported by the Coordenação de Aperfeiçoamento de Pessoal de Nível Superior (CAPES) (Ph.D. grant for EPM)−Brazil−Finance Code 001, and financial support was obtained from the Center for Interdisciplinary Nanostructure Science and Technology (CINSaT) of the University of Kassel.

Notes

The authors declare no competing financial interest.

■ ACKNOWLEDGMENTS

The authors acknowledge Pesque Pague Moinho (São Carlos, Brazil) for supplying the fresh skins of Nile Tilapia and the Institute of Materials Engineering for assistance with porosity and X-ray measurements.

■ REFERENCES

(1) Russ, W.; Meyer-Pittroff, R. Utilizing waste products from the food production and processing industries. *Crit. Rev. Food Sci. Nutr.* **2004**, *44*, 57−62.

(2) Veríssimo, N. V.; Mussagy, C. U.; Oshiro, A. A.; Mendonça, C. M. N.; Santos-Ebinuma, V. d. C.; Pessoa, A.; Oliveira, R. P. d. S.; Pereira, J. F. B. From green to blue economy: Marine biorefineries for a sustainable ocean-based economy. *Green Chem.* **2021**, *23*, 9377−9400.

(3) Villamil, O.; Váquiro, H.; Solanilla, J. F. Fish viscera protein hydrolysates: Production, potential applications and functional and bioactive properties. *Food Chem.* **2017**, *224*, 160−171.

(4) Wong, M.-H.; Mo, W.-Y.; Choi, W.-M.; Cheng, Z.; Man, Y.-B. Recycle food wastes into high quality fish feeds for safe and quality fish production. *Environ. Pollut.* **2016**, *219*, 631−638.

(5) Ideia, P.; Pinto, J.; Ferreira, R.; Figueiredo, L.; Spínola, V.; Castilho, P. C. Fish Processing Industry Residues: A Review of Valuable Products Extraction and Characterization Methods. *Waste Biomass Valorization* **2020**, *11*, 3223−3246.

(6) Sai-Ut, S.; Jongjareonrak, A.; Rawdkuen, S. Re-extraction, Recovery, and Characteristics of Skin Gelatin from Farmed Giant Catfish. *Food Bioprocess Technol.* **2012**, *5*, 1197−1205.

(7) Lin, K.; Zhang, D.; Macedo, M. H.; Cui, W.; Sarmento, B.; Shen, G. Advanced Collagen-Based Biomaterials for Regenerative Biomedicine. *Adv. Funct. Mater.* **2019**, *29*, No. 1804943.

(8) Dillard, C. J.; German, J. B. Phytochemicals: nutraceuticals and human health. *J. Sci. Food Agric.* **2000**, *80*, 1744−1756.

(9) Zuo, J.; Yin, Q.; Wang, L.; Zhang, W.; Fan, Y.; Zhou, Y.-Y.; Li, Y.; Wang, G.-D. Mangosteen ethanol extract alleviated the severity of collagen-induced arthritis in rats and produced synergistic effects with methotrexate. *Pharm. Biol.* **2018**, *56*, 455−464.

(10) Cheng, H.-Y.; Lin, T.-C.; Yu, K.-H.; Yang, C.-M.; Lin, C.-C. Antioxidant and free radical scavenging activities of *Terminalia chebula*. *Biol. Pharm. Bull.* **2003**, *26*, 1331−1335.

(11) Alves, N. M.; Leonor, I. B.; Azevedo, H. S.; Reis, R. L.; Mano, J. F. Designing biomaterials based on biomineralization of bone. *J. Mater. Chem.* **2010**, *20*, 2911−2921.

(12) Jiao, K.; Niu, L.-N.; Ma, C.-F.; Huang, X.-Q.; Pei, D.-D.; Luo, T.; Huang, Q.; Chen, J.-H.; Tay, F. R. Complementarity and Uncertainty in Intrafibrillar Mineralization of Collagen. *Adv. Funct. Mater.* **2016**, *26*, 6858−6875.

(13) Qiu, Z.-Y.; Cui, Y.; Tao, C.-S.; Zhang, Z.-Q.; Tang, P.-F.; Mao, K.-Y.; Wang, X.-M.; Cui, F.-Z. Mineralized Collagen: Rationale, Current Status, and Clinical Applications. *Materials* **2015**, *8*, 4733−4750.

(14) Hoyer, B.; Bernhardt, A.; Heinemann, S.; Stachel, I.; Meyer, M.; Gelinsky, M. Biomimetically mineralized salmon collagen scaffolds for application in bone tissue engineering. *Biomacromolecules* **2012**, *13*, 1059−1066.

(15) Yunoki, S.; Suzuki, T.; Takai, M. Stabilization of low denaturation temperature collagen from fish by physical cross-linking methods. *J. Biosci. Bioeng.* **2003**, *96*, 575−577.

(16) Milan, E. P.; Rodrigues, M. A. V.; Martins, V. C. A.; Plepis, A. M. G.; Fuhrmann-Lieker, T.; Horn, M. M. Mineralization of Phosphorylated Fish Skin Collagen/Mangosteen Scaffolds as Potential Materials for Bone Tissue Regeneration. *Molecules* **2021**, *26*, 2899.

(17) Tjahjani, S.; Widowati, W.; Khiong, K.; Suhendra, A.; Tjokropranoto, R. Antioxidant Properties of *Garcinia Mangostana* L (Mangosteen) Rind. *Procedia Chem.* **2014**, *13*, 198−203.

(18) Re, R.; Pellegrini, N.; Proteggente, A.; Pannala, A.; Yang, M.; Rice-Evans, C. Antioxidant activity applying an improved ABTS radical cation decolorization assay. *Free Radical Biol. Med.* **1999**, *26*, 1231−1237.

(19) Pal, J.; Ganguly, S.; Tahsin, K. S.; Acharya, K. *In vitro* free radical scavenging activity of wild edible mushroom, Pleurotus squarrosulus (Mont.) Singer. *Indian J Exp Biol.* **2010**, *48*, 1210−1218.

(20) Chen, Z.; Bertin, R.; Froldi, G. EC50 estimation of antioxidant activity in DPPH· assay using several statistical programs. *Food Chem.* **2013**, *138*, 414−420.

(21) Scherer, R.; Godoy, H. T. Antioxidant activity index (AAI) by the 2,2-diphenyl-1-picrylhydrazyl method. *Food Chem.* **2009**, *112*, 654−658.

(22) Horn, M. M.; Amaro Martins, V. C.; De Guzzi Plepis, A. M. *In Vitro* Mineralization Study of Chitosan/Carbon Nanotubes Scaffolds: Effect of Mineralization Cycles. *Macromol. Symp.* **2018**, *378*, No. 1600148.

(23) Pietrucha, K.; Safandowska, M. Dialdehyde cellulose-cross-linked collagen and its physicochemical properties. *Process Biochem.* **2015**, *50*, 2105−2111.

(24) Li, J.; Chen, Y.; Yin, Y.; Yao, F.; Yao, K. Modulation of nano-hydroxyapatite size via formation on chitosan-gelatin network film in situ. *Biomaterials* **2007**, *28*, 781−790.

(25) Rusu, V. M.; Ng, C.-H.; Wilke, M.; Tiersch, B.; Fratzl, P.; Peter, M. G. Size-controlled hydroxyapatite nanoparticles as self-organized organic-inorganic composite materials. *Biomaterials* **2005**, *26*, 5414−5426.

(26) Zarena, A. S.; Sankar, K. U. A study of antioxidant properties from *Garcinia mangostana L.* pericarp extract. *Acta Sci. Pol. Technol. Aliment.* **2009**, *8*, 23−34.

(27) Wittenauer, J.; Schweiggert-Weisz, U.; Carle, R. In vitro-study of antioxidant extracts from *Garcinia mangostana* pericarp and Riesling grape pomace − a contribution to by-products valorization as cosmetic ingredients. *J. Appl. Bot. Food Qual.* **2016**, *89*, 249−257.

(28) Suttirak, W.; Manurakchinakorn, S. *In vitro* antioxidant properties of mangosteen peel extract. *J. Food Sci. Technol.* **2014**, *51*, 3546−3558.

(29) Chaiwarit, T.; Kantrong, N.; Sommano, S. R.; Rachtanapun, P.; Junmahasathien, T.; Kumpugdee-Vollrath, M.; Jantrawut, P. Extraction of Tropical Fruit Peels and Development of HPMC Film Containing the Extracts as an Active Antibacterial Packaging Material. *Molecules* **2021**, *26*, 2265.

(30) Hu, Z.; Yang, P.; Zhou, C.; Li, S.; Hong, P. Marine Collagen Peptides from the Skin of Nile Tilapia (*Oreochromis niloticus*): Characterization and Wound Healing Evaluation. *Mar. drugs* **2017**, *15*, 102.

(31) Guo, M.; Wang, X.; Lu, X.; Wang, H.; Brodelius, P. E. α-Mangostin Extraction from the Native Mangosteen (*Garcinia mangostana* L.) and the Binding Mechanisms of α-Mangostin to HSA or TRF. *PLoS One* **2016**, *11*, No. e0161566.

(32) Abifarin, J. K.; Obada, D. O.; Dauda, E. T.; Dodoo-Arhin, D. Experimental data on the characterization of hydroxyapatite synthesized from biowastes. *Data Br.* **2019**, *26*, No. 104485.

(33) Júnior, Z. S. S.; Botta, S. B.; Ana, P. A.; França, C. M.; Fernandes, K. P. S.; Mesquita-Ferrari, R. A.; Deana, A.; Bussadori, S. K. Effect of papain-based gel on type I collagen–spectroscopy applied for microstructural analysis. *Sci. Rep.* **2015**, *5*, No. 11448.

https://doi.org/10.1021/acsomega.2c03266
ACS Omega 2022, 7, 34022−34033

(34) Fields, G. B. The collagen triple-helix: correlation of conformation with biological activities. *Connect. Tissue Res.* **1995**, *31*, 235−243.
(35) Sarrigiannidis, S. O.; Rey, J. M.; Dobre, O.; González-García, C.; Dalby, M. J.; Salmeron-Sanchez, M. A tough act to follow: collagen hydrogel modifications to improve mechanical and growth factor loading capabilities. *Mater. Today Bio* **2021**, *10*, No. 100098.
(36) Li, Q.; Mu, L.; Zhang, F.; Sun, Y.; Chen, Q.; Xie, C.; Wang, H. A novel fish collagen scaffold as dural substitute. *Mater. Sci. Eng., C.* **2017**, *80*, 346−351.
(37) Du, T.; Niu, X.; Hou, S.; Li, Z.; Li, P.; Fan, Y. Apatite minerals derived from collagen phosphorylation modification induce the hierarchical intrafibrillar mineralization of collagen fibers. *J. Biomed. Mater. Res., Part A* **2019**, *107*, 2403−2413.
(38) Wu, L.; Shao, H.; Fang, Z.; Zhao, Y.; Cao, C. Y.; Li, Q. Mechanism and Effects of Polyphenol Derivatives for Modifying Collagen. *ACS Biomater. Sci. Eng.* **2019**, *5*, 4272−4284.
(39) Daskalova, A.; Nathala, C. S.; Bliznakova, I.; Stoyanova, E.; Zhelyazkova, A.; Ganz, T.; Lueftenegger, S.; Husinsky, W. Controlling the porosity of collagen, gelatin and elastin biomaterials by ultrashort laser pulses. *Appl. Surf. Sci.* **2014**, *292*, 367−377.
(40) Abbasi, N.; Hamlet, S.; Love, R. M.; Nguyen, N.-T. Porous scaffolds for bone regeneration. *J. Sci.: Adv. Mater. Devices* **2020**, *5*, 1−9.
(41) Grabska-Zielińska, S.; Sionkowska, A.; Carvalho, Â.; Monteiro, F. J. Biomaterials with Potential Use in Bone Tissue Regeneration-Collagen/Chitosan/Silk Fibroin Scaffolds Cross-Linked by EDC/NHS. *Materials* **2021**, *14*, 1105.
(42) Al-Munajjed, A. A.; O'Brien, F. J. Influence of a novel calcium-phosphate coating on the mechanical properties of highly porous collagen scaffolds for bone repair. *J. Mech. Behav. Biomed. Mater.* **2009**, *2*, 138−146.
(43) Wang, J.; Liu, C. Biomimetic Collagen/Hydroxyapatite Composite Scaffolds: Fabrication and Characterizations. *J. Bionic Eng.* **2014**, *11*, 600−609.
(44) Câmara, G. I. F.; Menezes, M. d. L. L. R.; Vasconcelos, N. F.; Fechine, P. B. A.; Mattos, A. L. A.; Rosa, M. d. F.; de Souza Filho, M. d. S. M. Biocomposite based on nanoscale calcium phosphate and collagen from Nile tilapia (*Oreochromis niloticus*) skin: Properties and morphological features. *Mater. Lett.* **2020**, *279*, No. 128441.
(45) Wang, L.; Li, C. Preparation and physicochemical properties of a novel hydroxyapatite/chitosan−silk fibroin composite. *Carbohydr. Polym.* **2007**, *68*, 740−745.
(46) Dorozhkin, S. Nanodimensional and Nanocrystalline Apatites and Other Calcium Orthophosphates in Biomedical Engineering, Biology and Medicine. *Materials* **2009**, *2*, 1975−2045.
(47) Wan, Y.; Hong, L.; Jia, S.; Huang, Y.; Zhu, Y.; Wang, Y.; Jiang, H. Synthesis and characterization of hydroxyapatite−bacterial cellulose nanocomposites. *Compos. Sci. Technol.* **2006**, *66*, 1825−1832.
(48) Elhendawi, H.; Felfel, R. M.; Abd El-Hady, B. M.; Reicha, F. M. Effect of Synthesis Temperature on the Crystallization and Growth of In Situ Prepared Nanohydroxyapatite in Chitosan Matrix. *ISRN Biomater.* **2014**, *2014*, 1−8.

https://doi.org/10.1021/acsomega.2c03266
ACS Omega 2022, 7, 34022−34033